Semiclassical analysis of long-wavelength multiphoton processes: The Rydberg atom

Luz V. Vela-Arevalo* and Ronald F. Fox[†]

Center for Nonlinear Sciences and School of Physics, Georgia Institute of Technology, Atlanta, Georgia 30332-0430, USA
(Received 12 December 2003; published 15 June 2004)

We study the problem of multiphoton processes for intense, long-wavelength irradiation of atomic and molecular electrons. An exact, nonperturbative approach is applied to the standard vector potential coupling Hamiltonian for a three-dimensional hydrogenlike atom in a microwave field treated semiclassically. Multiphoton probability exchange is calculated in both the velocity and the length gauges, by applying the Goeppert-Mayer gauge transformation. The expansion of the time-dependent solution in terms of Floquet states delineates the mechanism of multiphoton transitions. A detailed analysis of the Floquet states and quasienergies as functions of the field parameters allows us to describe the relation between avoided quasienergy crossings and multiphoton probability exchange. We formulate analytical expressions for the variation of quasienergies and Floquet states with respect to the field parameters, and demonstrate that avoided quasienergy crossings are accompanied by dramatic changes in the Floquet states. Analysis of the Floquet states, for small values of the field strength, yields selection rules for the avoided quasienergy crossings. In the case of strong fields, the simultaneous choice of frequency and strength of the field producing an avoided crossing results in improved ionization probability.

I. INTRODUCTION

Multiphoton processes involving atomic and molecular electrons have been widely studied both in experiments and in different theoretical treatments, some of which are directly related to questions of quantum chaos [1–3]. The goal of this work is to study dynamical features of multiphoton transitions in the three-dimensional hydrogenlike Rydberg atom in a semiclassical radiation field. The problem is studied by direct integration of the system of ordinary differential equations (ODE's) resulting from expanding the time-dependent solution in terms of a finite basis of unperturbed states. With this approach, we describe the effect of the Goeppert-Mayer gauge transformation [4], that is, we calculate the wave function for the standard vector potential coupling Hamiltonian (in the velocity gauge [5]) and for the electric dipole Hamiltonian (length gauge [5]). We compute time-evolving probabilities and their strong dependence on field parameters. We are focused on field frequencies close to unperturbed resonances, which in general interfere with results obtained from perturbative methods.

A detailed analysis of the Floquet quasienergies and Floquet states for the Rydberg Hamiltonian allows us to describe their role in multiphoton probability exchange. We provide analytical expressions of the variation of Floquet states and quasienergies as a function of the field parameters (strength and frequency). This analysis provides the basis for the understanding of the effects of avoided quasienergy crossings on probability exchange. We show that avoided quasienergy crossings are accompanied by dramatic changes in the components of the Floquet states, which may feature probability exchange. With this analysis we can predict transition rates and selection rules for multiphoton transitions. The analytic

and numerical techniques presented in this work are nonperturbative and can be extended to general Rydberg atoms.

In the study of multiphoton processes due to a radiation field, often perturbative methods have been attempted, which are based mainly on the reduction of the problem to a two-level system (see, for instance, Refs. [5,6], and references therein). Naturally, low-order transition probability is only justified for the case of a weak field and for frequencies that are far from resonance, since the formulas have small denominators for resonant frequencies. The problem of intrashell dynamics has attracted attention since experiments in Ref. [2] suggest that intrashell dynamics is responsible for enhancement of ionization probability; in Ref. [7], intrashell dynamics is treated as two two-level problems. For the problem of a strong field, nonperturbative methods have been attempted, based on Floquet analysis introduced by Shirley [8]. With this approach, the Floquet states are obtained in the Fourier domain, and the problem is reduced to an eigenvalue problem for a time-independent infinite-dimensional matrix. Successful applications of this method can be found in Refs. [9,10]. In Ref. [11], there is a comparison between one- and two-dimensional probability transitions of the Rydberg Hamiltonian. Also for the Rydberg problem, multiphoton transitions are studied in Refs. [12,13] under the influence of both a microwave and a static field. Their analysis is based on Floquet states obtained by Blochinzew [14]. These Floquet states, however, are obtained within an n shell of a Rydberg Hamiltonian under a microwave field, in which nondiagonal matrix elements between states with different principal quantum number n have been neglected. We are interested in the Floquet analysis of the fully coupled Hamiltonian, and we describe the dynamics of the system in the time domain, that is, we provide the time evolution of the transition probabilities as a consequence of the expansion of the solution in terms of Floquet states.

The radiation wavelength under consideration in this work is much larger than the spatial extent of the electron

---

*Electronic address: luzvela@cns.physics.gatech.edu
[†]Electronic address: ron.fox@physics.gatech.edu

69 063409-1

states even for high n. Therefore, the dipole approximation [15] applies and the field is independent of the spatial coordinates. We provide examples of multiphoton transitions in two regimes: transitions from the ground state to excited states of hydrogen and transitions between excited Rydberg states that are close to ionization. The same approach provided a negative proof for the existence of multiphoton transitions for the periodically driven simple harmonic oscillator [16].

We obtain analytical expressions for the variation of the quasienergies and Floquet states as functions of the field parameters. These expressions are analogs of some expressions obtained in Ref. [17] in a different context. When the field parameters vary, both crossings and avoided crossings of the quasienergies can be observed. Our analysis permits us to demonstrate that, when the quasienergies feature an avoided crossing, the Floquet states show dramatic changes. As a consequence, the time-dependent solution can be obtained as the superposition of two or more Floquet states, which results in probability exchange between unperturbed states when the radiation field is present. When a crossing occurs, the Floquet states are not significantly affected since the solution may be expanded in terms of mainly one Floquet state, hence there is no transition probability. The dynamics close to avoided crossings was also studied in Ref. [18]; however, our analytic results are different and explain the numerical observations.

For small values of the field strength, the Floquet states are very close to unperturbed states. This is used to obtain selection rules for the avoided quasienergy crossings. For a transition of N photons, an avoided crossing is possible if the states involved have a difference in quantum number l that is even for N even or odd for N odd. We provide an expression for the rate of transition for these cases, which is inversely related to the difference in the quasienergies involved in the avoided crossing. As the field strength varies, the values of the field frequency producing avoided crossings also vary (a consequence of the ac or dynamic Stark effect [6]). This shows that the tuning of the field parameters should be done simultaneously to achieve an optimal transition.

The paper is organized as follows. In Sec. II we review the Hamiltonian of the Rydberg atom in a microwave field, in both the velocity and length gauges, which are related by the Goeppert-Mayer gauge transformation. The solution is expanded in terms of unperturbed states; the dynamics is then reduced to the auxiliary equations. Examples of multiphoton transitions from the ground state are presented in Sec. III; the time-evolving probabilities are obtained in both velocity and length gauges by computing the effect of the Goeppert-Mayer gauge transformation. Floquet analysis of the auxiliary equations and the computation of Floquet states and quasienergies is described in Sec. IV; through examples, we describe long-term dynamical features that can be obtained from the expansion of the initial condition in terms of Floquet states at $t=0$. We explore, analytically, the behavior of quasienergies and Floquet states close to avoided crossings as the parameters vary in Sec. V. The study of the Floquet states as a function of the parameters allows us to identify selection rules for multiphoton transitions; this is described in detail in Sec. VI. The conclusions and discus-

sion is in Sec. VII. Finally, in Appendix A, we give heuristic reasons for the existence of multiphoton resonances by studying the Laplace transform of the auxiliary equations.

II. THE RYDBERG-ATOM HAMILTONIAN

The Hamiltonian for the Rydberg atom in an intense semiclassical microwave radiation field is given by

$$H = \frac{1}{2m_e}\left(\vec{p} + \frac{e}{c}\vec{A}(t)\right)^2 - \frac{e^2 Z}{r}. \tag{1}$$

The microwave field $\vec{A}$ with amplitude A_0 and frequency ω is given by

$$\vec{A}(t) = A_0\hat{\varepsilon}\,\sin(\omega t),$$

in which $\hat{\varepsilon}$ is the polarization unit vector. The electron charge is $-e$, $e > 0$.

Applying the Goeppert-Mayer gauge transformation [4,5,19]

$$\chi(\vec{r},t) = -\frac{ie}{\hbar c}\vec{r}\cdot\vec{A}(t), \tag{2}$$

the Hamiltonian (1) is related to the electric dipole Hamiltonian given by

$$\widetilde{H} = H_0 + e\vec{r}\cdot\vec{E}, \tag{3}$$

where H_0 is the unperturbed Hamiltonian for a hydrogenlike atom,

$$H_0 = \frac{p^2}{2m_e} - \frac{e^2 Z}{r}, \tag{4}$$

and $\vec{E} = -(1/c)(\partial\vec{A}/\partial t)$ is the electric field.

The Hamiltonian (1) is in the so-called *velocity gauge* [5]. The dipole Hamiltonian (3) is given in the so-called *length gauge* [5]. The corresponding wave functions ψ of Eq. (1) and $\widetilde{\psi}$ of Eq. (3) are related by

$$\psi(\vec{r},t) = \exp\left(-\frac{ie}{\hbar c}\vec{r}\cdot\vec{A}(t)\right)\widetilde{\psi}(\vec{r},t). \tag{5}$$

Let the time-dependent solution of Eq. (3) be expanded as

$$|\widetilde{\psi}(t)\rangle = \sum_k a_k(t)|\phi_k\rangle, \tag{6}$$

where $|\phi_k\rangle$ are the unperturbed states of Eq. (4), i.e.,

$$H_0|\phi_k\rangle = E_k|\phi_k\rangle. \tag{7}$$

Substituting Eq. (6) in the Schrödinger equation, it can be shown that the coefficients $a_k(t)$ must satisfy auxiliary equations given by

$$\frac{da_k}{dt} = -i\frac{E_k}{\hbar}a_k + i\sum_j \frac{e}{\hbar c}\left(\frac{d}{dt}\vec{A}\right)\cdot\langle\phi_k|\vec{r}|\phi_j\rangle a_j. \tag{8}$$

The details of the derivation of the auxiliary equations can be found in Ref. [16]. The derivation applies for any central

force problem. For the calculations in this work, we consider the hydrogen atom Hamiltonian, that is, $Z=1$ in Eq. (4). For hydrogenlike atoms, the indices k and j in Eq. (8) are actually triples, corresponding to the quantum numbers n, l, m. The principal quantum number n is a positive integer; $l=0,\ldots,n-1$, and $m=-l,\ldots,l$. The energies are given by $E_k=-E_I/n^2$, where $E_I=e^2/2a_0$ (erg) is the ionization energy and n is the principal quantum number of the corresponding state. The polarization direction of the microwave field is taken as the z axis, i.e., $\hat{\varepsilon}=\hat{k}$. The vector potential is expressed as $\vec{A}(t)=A_0\hat{k}\sin(\omega t)$. Normalizing coordinates and constants by atomic quantities, the auxiliary equations (8) are expressed in dimensionless units as

$$\frac{da_k}{dt}=-i\omega_k a_k+i\lambda\,\cos(\omega t)\sum_j\langle\phi_k|z|\phi_j\rangle a_j,\qquad(9)$$

where $\omega_k=\omega_n=-1/2n^2$ (n is the principal quantum number of the corresponding state), $\lambda=E_0/(5.1422\times10^9\ \text{V/cm})$, and $E_0=\omega A_0/c$. The matrix elements are known in close form [20]. The matrix elements $\langle\phi_k|z|\phi_j\rangle$ imply two selection rules:

$$m'=m\quad\text{and}\quad l'=l\pm1.\qquad(10)$$

The auxiliary equations (9) form a nonautonomous, linear, time-periodic system of ODE's. In the Appendix we study the Laplace transform of the system to obtain driving field frequencies that may cause secularities, and it is immediately obvious that an analytical solution is difficult to achieve, even for a small number of states. Equations (9) form an infinite-dimensional system. The analysis is done for a truncated system of equations or a finite basis of unperturbed states. The selection rules (10) imply that the quantum number m of the interacting states is fixed by the initial condition (initial state). The basis is formed by states in a finite set of principal quantum numbers n; the value of m fixes the minimum n to $|m|+1$. All coupled l substates ($l=|m|,\ldots,n-1$) were included. The coupling term is larger between coefficients with the same principal quantum number n, and decreases as the difference $n'-n$ increases. However, our computations show that the probability may spread to many states, both within the same n and to states with different n. Even small couplings can have a long-term effect, and therefore the integration must consider states within a large number of energy levels to avoid saturation. In our numerical experiments, the maximum n was determined to have the higher states with negligible probability. Ionization probability is computed as the probability above an $\bar{n}$ cutoff value [3], which has to be smaller than the maximum n in the simulations. However, in strict terms, ionization probability must include the probability of continuum states, which are not considered here. Including the continuum states as well as increasing the basis size to infinity may result in a dense spectrum [18].

The choice of ω, the frequency of the microwave field, provides the mechanism to effectively couple the initial state with some excited state. From the Laplace transform of these
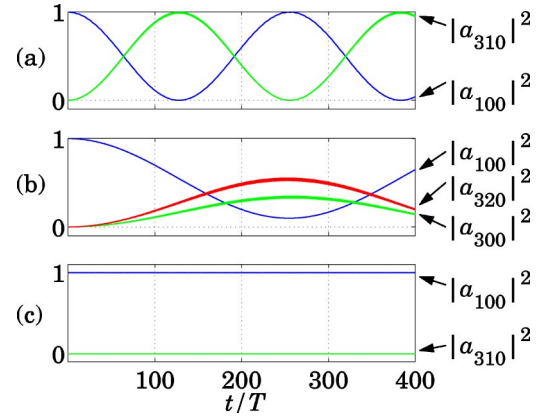

FIG. 1. (Color online) Evolution of the squared absolute value of some coefficients $a_k(t)$ for three different values of the driving frequency: (a) $\omega=\omega_3-\omega_1$, (b) $\omega=(\omega_3-\omega_1)/2$, and (c) $\omega=(\omega_3-\omega_1)/[(1+\sqrt{5})/2]$. In all cases, the initial condition is $a_{100}(0)=1$ and zero for the rest. $\lambda=0.005\,861\,7$. There is probability exchange only in the resonant cases (a) and (b), between the ground state ($n=1$) and excited states with $n=3$. The time t (in atomic unit) was normalized in each case by the value of the respective period ($T=2\pi/\omega$).

equations (see the Appendix), we concluded that secularities arise with frequencies ω satisfying equations of the form

$$\omega_j-\omega_k\pm N\omega=0,$$

where N is an integer. Numerical experiments showed that choosing ω satisfying (closely) this equation is key to produce multiphoton transitions between the states with frequencies ω_j and ω_k, with N the number of photons involved in the transition.

Based on Floquet analysis, we later establish that the values of ω producing multiphoton transitions should be chosen simultaneously with the parameter λ, the strength of the field. λ can be used as a tuning parameter for the rate of transition. However, as we show in the following section, the dependence of the transition rate with respect to λ is rather complicated.

III. MULTIPHOTON TRANSITIONS

Three examples of solution of the auxiliary equations (9) are shown in Fig. 1. We took the ground state as the initial condition [$a_{100}(0)=1$ and zero for all others], and obtained probability exchange with excited states. We fixed the value of $\lambda=0.005\,861\,7(=3.01\times10^7\ \text{V/cm})$ and evolved the system for three different values of the coupling frequency: (a) $\omega=\omega_3-\omega_1$, (b) $\omega=(\omega_3-\omega_1)/2$, and (c) $\omega=(\omega_3-\omega_1)/[(1+\sqrt{5})/2]$. For the case (a), we observed Rabi-type oscillations between the states $|1,0,0\rangle$ and $|3,1,0\rangle$, alternating in probability to *almost* 100%; there is a small percentage of probability spreading to other states. The first transition takes about 125 periods of the external field. Meanwhile for the case (b), two excited coefficients appear: the probability oscillates between the ground state, and the states $|3,2,0\rangle$ and $|3,0,0\rangle$. The first transition occurs after 250 field periods. On
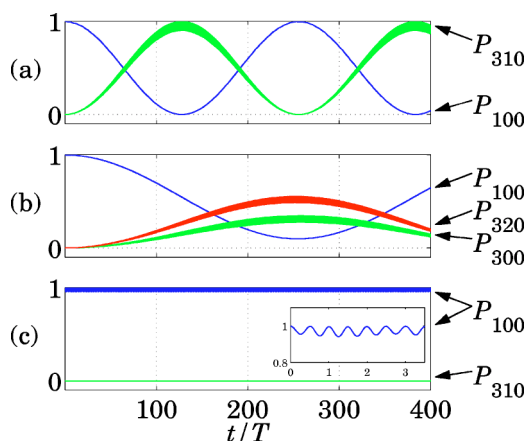
FIG. 2. (Color online) Time evolution of the probabilities $P_k(t)$ [Eq. (11)]. The parameters are the same as in Fig. 1: (a) $\omega = \omega_3 - \omega_1$, (b) $\omega = (\omega_3 - \omega_1)/2$, and (c) $\omega = (\omega_3 - \omega_1)/[(1 + \sqrt{5})/2]$. In all cases, $\lambda = 0.005\ 861\ 7$.

the other hand, in the nonresonant case (c), the probability remains in the coefficient a_{100} with small oscillations around it. There is no transition in this case.

Goeppert-Mayer gauge transformation

The solution of the auxiliary equations (9) provides the evolution of the system in the length gauge (3) in the form (6). In order to obtain a time-dependent solution of the vector potential coupling Hamiltonian (1), we need to apply the Goeppert-Mayer gauge transformation (2). Recall that the wave functions are related by Eq. (5).

Hence, in the velocity gauge, the time-dependent solution (in spherical dimensionless coordinates) has the form

$$|\psi(t)\rangle = \exp\left[-\frac{i\lambda}{\omega} r \cos\theta \sin(\omega t)\right] \sum_j a_j(t) |\phi_j\rangle.$$

The probability of finding the electron in an unperturbed state $|\phi_k\rangle$ at time t is given by

$$P_k(t) = |\langle \phi_k | \psi(t)\rangle|^2 = \left| \sum_j a_j(t) M_{k,j}(t) \right|^2, \qquad (11)$$

where

$$M_{k,j}(t) = \langle \phi_k | \exp\left[-\frac{i\lambda}{\omega} r \cos\theta \sin(\omega t)\right] |\phi_j\rangle$$

$$= 2\pi \int_0^\infty \int_0^\pi e^{(-i\lambda/\omega)r \cos\theta \sin(\omega t)} \phi_k^* \phi_j r^2 \sin\theta\, dr\, d\theta.$$

$$(12)$$

For the same parameters as in Fig. 1, the evolution of the probabilities is shown in Fig. 2.

The computation of probability evolution requires the evaluation of the matrix elements (12) for all $t \in [0, T]$. (Note that the integral over the angle φ has been evaluated assuming that $m = m'$.) For most cases, this double integral can only be evaluated numerically. In a few cases with low quantum
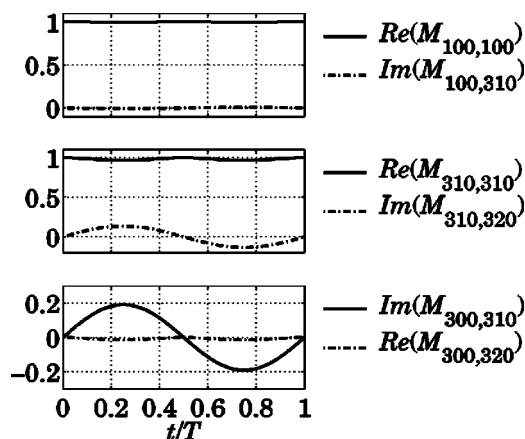
numbers n and n' the integral can be evaluated using symbolic computation software such as MATHEMATICA. But even the numerical integration is difficult due to the fast oscillations of the integrand, as we observed in some attempts to use MATHEMATICA, which produced inaccuracies. We tried to overcome this with our own FORTRAN code using Gaussian integration over θ and Laguerre integration over r [21]. We sampled time points in the interval $[0, T/4]$, and by symmetry obtained sampled values of the matrix elements over one period $[0, T]$. The evaluation for any $t \in [0, T]$ was then obtained by interpolation. For the total integration time of $400T$, we can use the periodicity of the matrix elements: $M_{k,j}(t + T) = M_{k,j}(t)$.

Examples of some matrix elements (12) corresponding to low quantum numbers are shown in Fig. 3. In general, the matrix element is real if $l - l'$ is even, and purely imaginary if the difference in l is odd. The parameters used in this figure are the same as in the example of Fig. 1(b): $\omega = (\omega_3 - \omega_1)/2$ and $\lambda = 0.005\ 861\ 7$. We notice that for low principal quantum numbers the matrix elements $M_{k,j}$ are close to 1 for $k = j$ and close to 0 otherwise.

Having computed the coefficients $a_k(t)$ and the matrix elements $M_{k,j}(t)$, we are able to obtain the time-dependent solution and probability evolution. From Fig. 3, we observe that $\langle \phi_k | \psi(t)\rangle \approx a_k(t)$. Then, the evolution of probabilities (11) for this choice of parameters and initial condition is very similar to the evolution of the coefficients $a_k(t)$. Compare Figs. 1 and 2.

Figure 2(a) represents a 1-photon transition between the levels 1 and 3 with almost 100% of probability exchange; the probability oscillates in time, in a similar way of a Rabi oscillation; however, there is a small percentage of probability going to other states, which shows the effect of the multiple coupled states. Meanwhile, (b) reflects a 2-photon transition between the ground state and $|3,0,0\rangle$ with probability of at most 30% and $|3,2,0\rangle$ with at most 60%. Again, the probability oscillates in time, after about 508 periods of the field the ground state has probability close to 100%. In these figures, very quick small oscillations make the lines look thick, as it is depicted in the inset of Fig. 2(c).

Now, we study multiphoton transitions between states in the levels $n = 1$ and $n = 8$ as a function of the field strength.
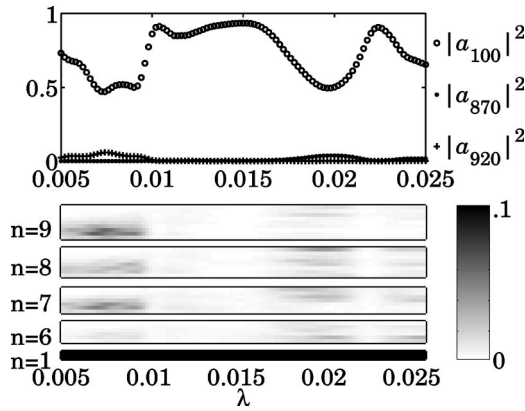

FIG. 3. Some matrix elements $M_{k,j}(t)$ [Eq. (12)] for $\omega = (\omega_3 - \omega_1)/2$ and $\lambda = 0.005\ 861\ 7$.

FIG. 4. Time and initial phase averaged probabilities for $\omega_8 - \omega_1 - 8\omega = 0$ and varying λ, over a fixed time interval of $400T$. In the lower panels we see the distribution of averaged probabilities among several states with quantum numbers n indicated. Darker areas correspond to larger probabilities.

We integrate the auxiliary equations (9) for the fixed value of field frequency $\omega = (\omega_8 - \omega_1)/8$ and values of λ in the range 0.005 and 0.025 ($\approx 2.5 \times 10^7$ to 1.28×10^8 V/cm). The initial condition was chosen with all the probability on the ground state, i.e., $a_{100}(0) = 1$ and all other coefficients zero. Equations (9) were integrated over a fixed interval of time of $400T$, $T = 2\pi/\omega$ and for different initial phases. For each λ we computed the time and initial phase average of the probability in each state, that is, the average of $|a_k(t)|^2$ over $400T$.

In the first panel of Fig. 4 we show the time and initial phase averages of $|a_{100}|^2$, $|a_{870}|^2$, and $|a_{920}|^2$ as a function of λ. The graph in the second panel shows the distribution of the averaged probability as a function of λ. The gray scale is the averaged probability for each state with quantum numbers $n = 1, 6, 7, 8, 9$. In each n band, the vertical axis corresponds to the index l of the coefficients a_{nl0}; this is, $l = 0, \ldots, n-1$ (note that the vertical size increases for larger n, only because there are n levels represented in each band). The darker gray zones correspond to greater values.

We can observe in Fig. 4 that for values of λ around 0.008 and 0.02, the probability of the ground state averages 0.5; there is an exchange of probability between the ground state and several states with quantum numbers $n = 7, 8, 9$, and 10. This shows that although the field frequency ω is in resonance with states $n = 1$ and $n = 8$, the probability does not exchange only between those states (the reduction to a two-level system does not hold), but it can disperse in neighboring states in same n shell and other n shells. It is also noticeable that the relation between λ and the transition probability is quite complicated, and by no means linear.

In Fig. 5, we show the time evolution of some probabilities (11) for $\omega = (\omega_8 - \omega_1)/8$ and $\lambda = 0.008\,389$. We can see that, after ≈ 90 periods of the field, the probability of finding the electron in the ground state is zero. At that time, several states with $n = 7$, $n = 8$, and $n = 9$ have nonzero probability; the state $|9, 2, 0\rangle$ is the one with largest probability at this point. In all these states, the probability is oscillating rapidly, as we can observe in the insets of Fig. 5.

We also note that the Goeppert-Mayer gauge transformation has important effects for the case of excited states. In
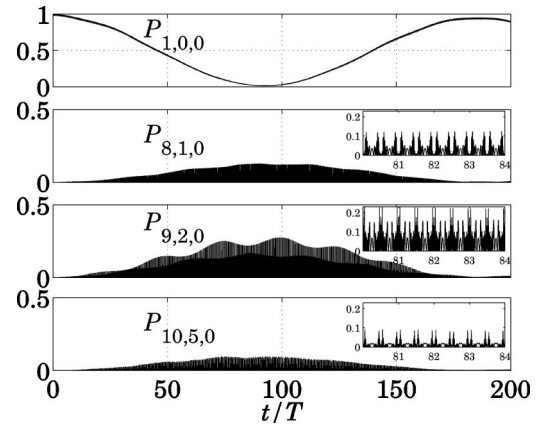

FIG. 5. Probabilities $P_k(t)$ [Eq. (11)] for $\omega_8 - \omega_1 - 8\omega = 0$ and $\lambda = 0.008\,389$. The insets provide the fine detail of the quick oscillations.

Fig. 6 we plot some matrix elements $M_{k,j}(t)$ that are needed to compute the probabilities [see Eqs. (11) and (12)]. Compare with the case of lower n's quantum numbers in Fig. 2.

IV. FLOQUET ANALYSIS

In this section, we calculate quantum Floquet states and quasienergies for the Rydberg Hamiltonian (1). One of the main advantages of the treatment discussed in this work is that the Floquet analysis of the auxiliary equations (9) (a system of ordinary differential equations) produces Floquet states for the quantum problem. It can be shown [22] that the Floquet exponents μ of the auxiliary equations are the Floquet quasienergies of the quantum system. Also, the Floquet solutions $a^\mu(t)$ yield quantum Floquet states defined by the expansion (6) in terms of unperturbed states (7). Note that each Floquet solution $a^\mu(t)$ is a vector of coefficients $a_k^\mu(t)$.

The auxiliary equations (9) for the coefficients $a_k(t)$ form a time-periodic system, with period $T = 2\pi/\omega$. Therefore, it is possible to find a basis of solutions $a^{\mu_m}(t)$, called the Floquet solutions, of the form
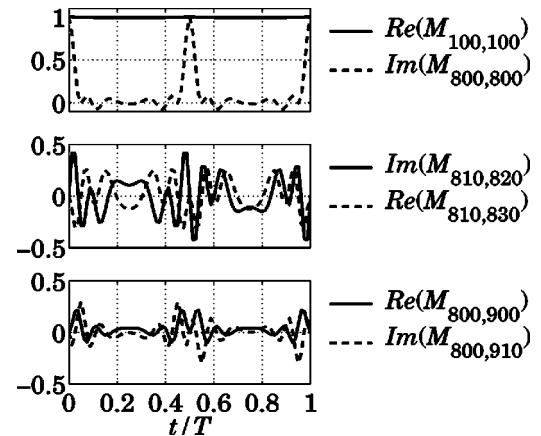

FIG. 6. Some matrix elements (12) for $\omega = (\omega_8 - \omega_1)/8$ and $\lambda = 0.008\,389$.

$$a^{\mu_m}(t) = e^{-i\mu_m t}x_m(t), \tag{13}$$

where μ_m is called the Floquet exponent and $x_m(t)$ is a vector of T-periodic functions. Any vector solution $a(t)$ can be expressed as a superposition of Floquet solutions [23], such as

$$a(t) = \sum_m c_m a^{\mu_m}(t). \tag{14}$$

The Floquet solutions yield Floquet states for the Hamiltonian (1) of the form

$$|\psi^{\mu_m}(t)\rangle = \exp\left(-\frac{i\lambda}{\omega}z\,\sin(\omega t)\right)\sum_k a_k^{\mu_m}(t)|\phi_k\rangle, \tag{15}$$

where $|\phi_k\rangle$ are the unperturbed states (7). The Floquet exponents μ_m are called the *quasienergies* of the Hamiltonian (1). Therefore, any time-dependent solution of the Hamiltonian (1) can be expressed as a superposition of Floquet states,

$$|\psi(t)\rangle = \sum_m c_m|\psi^{\mu_m}(t)\rangle. \tag{16}$$

The Floquet solutions a^{μ_m} are obtained from the monodromy matrix. Let $\Phi(t,t_0)$ be the matrix of fundamental solutions of the auxiliary equations (9) with $\Phi(t_0,t_0)=\mathbb{1}$, that is, any solution $a(t)$ with initial condition $a(t_0)=a_0$ is given by $a(t)=\Phi(t,t_0)a_0$. For simplicity, let $t_0=0$. The monodromy matrix is $\Phi(T,0)$. The eigenvalues of the monodromy matrix are the Floquet multipliers. If σ_m is a Floquet multiplier, the Floquet exponent μ_m is defined by $\sigma_m=e^{-i\mu_m T}$. The Floquet exponent μ_m is obtained modulo ω, that is, $\mu_m =[-i\ln(\sigma_m)/T]\mathrm{mod}\,\omega$. The Floquet solution is given by $a^{\mu_m}(t)=\Phi(t,0)x_m(0)$, where $x_m(0)$ is the eigenvector corresponding to the exponent μ_m. Furthermore, a^{μ_m} has the form (13). Note, from expression (16), that the coefficients c_m are constants, which are determined by the initial condition. At $t=0$, the Floquet states (15) correspond to an expansion in terms of unperturbed states. The coefficients of this expansion are given by $a_k^{\mu_m}(0)$. Now, from expression (13), these coefficients are precisely the components of the eigenvectors $x_m(0)$. We compute the monodromy matrix $\Phi(T,0)$ of the auxiliary equations (9) by direct numerical integration, that is, we integrate Eq. (9) taking as initial conditions each of the columns of the identity matrix $\mathbb{1}$, over a time interval of one period $[0,T]$. Then, we are able to compute eigenvalues and eigenvectors with which we can construct the quantum Floquet states.

Probability exchange from superposition of Floquet solutions

In Fig. 7, we plot the first 15 Floquet quasienergies for the same parameters previously studied in the examples in Figs. 1 and 2. The labeling of the quasienergies is arbitrary; we called them μ_m for $m=1,\ldots,15$ in increasing order. We note that for the resonant cases (a) and (b) all the quasienergies are close to the unperturbed energies $\omega_n=-1/(2n^2)$. However, the quasienergies in the same n shell have split and the degeneracies disappeared. In the resonant cases, there are four quasienergies (μ_3 to μ_6) which are close to ω_3. This "additional" quasienergy splitting from ω_3 is the quasienergy
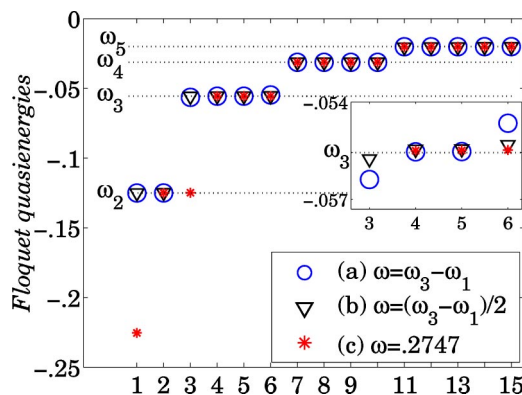

FIG. 7. (Color online) First 15 Floquet quasienergies μ_m for three different frequencies of the driving field. The strength of the field is fixed, $\lambda=0.005\,861\,7$. The lines labeled with the unperturbed energies ω_n are plotted for reference.

corresponding to ω_1, since $\omega_1 \mathrm{mod}\,\omega\equiv\omega_3$ [that is, $\omega_1=\omega_3 -N\omega$, with $N=1$ for (a) and $N=2$ for (b)]. On the other hand, for the nonresonant case (c), with $\omega=(\omega_3-\omega_1)/[(1+\sqrt{5})/2] =0.2747$, the Floquet quasienergy μ_1 is close to $\omega_1\,\mathrm{mod}\,\omega \equiv-0.5+0.2747=-0.2253$.

Let us discuss with more detail the resonant case (a) in Fig. 7. Let the initial condition be the ground state, that is, at $t=0$, $a_{100}(0)=1$, and the other coefficients zero. This initial condition is expanded, almost exactly, in terms of only two eigenvectors: the eigenvectors corresponding to the quasienergies μ_3 and μ_6 (Fig. 7). Recall that, at $t=0$, the components of the eigenvectors are coefficients of the unperturbed states. The components of these eigenvectors are illustrated in Fig. 8(a). Therefore, the evolution of the coefficient a_{100} can be approximated by

$$a_{100}(t) \approx c_3 e^{-i\mu_3 t}x_3^{100}(t) + c_6 e^{-i\mu_6 t}x_6^{100}(t),$$

where $x_3(t)$ and $x_6(t)$ are vectors of T-periodic functions and only their first component $(k=1,0,0)$ appears. At multiples
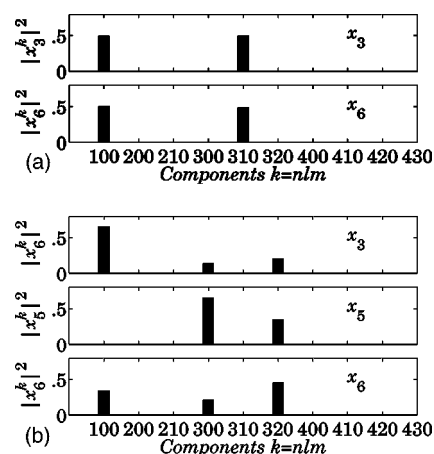

FIG. 8. Squared modulus of the components of eigenvectors corresponding to quasienergies (a) μ_3 and μ_6, with $\omega=\omega_3-\omega_1$ and (b) μ_3, μ_5, and μ_6 with frequency $\omega=(\omega_3-\omega_1)/2$ [see Figs. 7(a) and 7(b)]. $\lambda=0.005\,861\,7$.

of the period, $t=KT$, the functions $x_3(t)$ and $x_6(t)$ are precisely the eigenvectors represented in Fig. 8(a). For this case, $|c_3|^2=0.4922$ and $|c_6|^2=0.5064$. When evaluated at multiples of the period $t=KT$, $|a_{100}(KT)|^2$ is the probability of finding the electron in the $|1,0,0\rangle$ state. That is, $|a_{100}(KT)|^2 = |\langle 1,0,0|\psi(KT)\rangle|^2$ since the Goeppert-Mayer gauge transformation is the identity at those points. We can then find that this probability evolves as

$$|a_{100}(KT)|^2 \approx |c_3 e^{-iKT\mu_3}x_3^{100} + c_6 e^{-iKT\mu_6}x_6^{100}|^2.$$

Expanding the previous expression, we get

$$|a_{100}(KT)|^2 \approx |c_3 x_3^{100}|^2 + |c_6 x_6^{100}|^2 + 2 \cos[KT(\mu_6 - \mu_3)]$$
$$\times \text{Re}[c_3 c_6^* x_3^{100}(x_6^{100})^*].$$

Then, this probability evolves as a Rabi-type oscillation. The K-dependent term has a minimum for

$$K = \frac{\omega}{2(\mu_6 - \mu_3)}. \tag{17}$$

Evaluating, we get $K=127.8$. This is the number of periods of the microwave field for which the probability will have a maximum transition; in other words, this is half the period of the Rabi oscillation. The approximation above gives $|a_{100}(KT)|^2=0.4984+0.4983 \cos[KT(\mu_6-\mu_3)]$, then the maximum probability of the ground state after 1 period can be calculated as 99.67%. The remaining fraction of probability spreads to other coupled states. With the same argument we can obtain the probability $|a_{310}(KT)|^2=0.4902 -0.4902 \cos[KT(\mu_6-\mu_3)]$. The maximum probability for the state $|3,1,0\rangle$ is 98.04%. See Fig. 1(a).

In general, if the initial condition can be expanded in terms of mainly two Floquet states, the probabilities evolve as a Rabi-type flopping, and the quasienergies and Floquet states provide a very good approximation to the rate of oscillation and probability exchange. Note, however, that although only two quasienergies and Floquet states participate in the expansions of probability evolution, the system is not equivalent to a two-level system. The Floquet analysis was done considering all the coupled states. Simplification to a two-level system could not account for the fraction of probability that goes to other states.

On the other hand, for the resonant case (b) in Fig. 7, the initial condition $a_{100}=1$ (and the rest zero) is expanded in terms of mainly three eigenvectors, corresponding to the quasienergies μ_3, μ_6, and μ_5. The main coefficients in the Floquet expansion are $|c_3|^2=0.6566$, $|c_6|^2=0.3411$, $|c_5|^2 =0.0019$. In Fig. 8(b), the components of the eigenvectors are represented. From the components of the eigenvectors, we see that three unperturbed states participate: $|1,0,0\rangle$, $|3,0,0\rangle$, and $|3,2,0\rangle$. This produces the exchange of probability from the ground state $|1,0,0\rangle$ and those two excited states. Since two of the quasienergies μ_3 and μ_6 participate mostly in the expansion of the initial condition, we can still use expression (17) to approximate the rate of transition of the ground state as 254.3 field periods; this is the point at which the ground state reaches the minimum probability of 9.95%. [See Fig. 1(b).]

The previous analysis was repeated for several values of λ in the range 1×10^{-5} and 0.1 ($\approx 5\times 10^4$ and 5×10^8 V/cm). The quasienergies deviate more from the unperturbed energies as λ increases. This accounts for shorter period of the probability oscillation [see expression (17)]. For larger λ, the expansion of the ground state (initial condition) in terms of Floquet states involves more significant coefficients c_m. Also, the Floquet states are expressed in terms of more unperturbed states. This means that the probability spreads among more unperturbed states.

In the following sections, we analyze the cases when the initial condition is an excited Rydberg state, with quantum number $n>60$. In contrast with transitions involving the ground state and other low levels, where the energy gaps are well differentiated by n, in the case of $n>60$ the energy gaps are smaller and closer; therefore the resonances tend to overlap. We observe that for excited levels, the Floquet analysis yields a quite complicated behavior that is very sensitive to parameters. We present a detailed analysis of the variation of Floquet states and quasienergies with respect to parameters λ, ω.

V. FLOQUET ANALYSIS AS A FUNCTION OF PARAMETERS

The Hamiltonians for the Rydberg atom (1) and electric dipole (3) are related by the Goeppert-Mayer gauge transformation (2). Note that, at times multiple of the period, $t =KT$, the solutions for both Hamiltonians coincide [see expression (5)]. Particularly, the Floquet quasienergies also coincide, since they are computed as the eigenvalues of the monodromy matrix $\Phi(T,0)$ [see Sec. IV].

The Hamiltonian (3) is equivalent to the *Floquet Hamiltonian* in the extended phase space given by

$$\hat{K} = H_0 - z\lambda \cos \theta + \omega I, \tag{18}$$

where (θ,I) is an additional pair of canonical conjugate variables, and quantum mechanically, $I=-i\hbar \partial/\partial \theta$.

The Floquet Hamiltonian $\hat{K}$ can be diagonalized as

$$\hat{K}|\psi_m\rangle = \mu_m|\psi_m\rangle. \tag{19}$$

The eigenvalues μ_m coincide with the Floquet quasienergies [8]. The eigenstates are the quantum Floquet states $|\psi^{\mu_m}\rangle$ in the extended phase space.

A. Quasienergies and Floquet states as a function of λ

We now consider variations with respect to the parameter λ, the strength of the microwave field. Taking the derivative with respect to λ of Eq. (19), and using the orthonormality of the basis $|\psi_m\rangle$, we obtain (cf. Ref. [17])

$$-\langle\psi_n|z \cos \theta|\psi_m\rangle + \mu_n\langle\psi_n|\frac{d}{d\lambda}|\psi_m\rangle$$

$$= \frac{d\mu_m}{d\lambda}\delta_{mn} + \mu_m\langle\psi_n|\frac{d}{d\lambda}|\psi_m\rangle.$$

Then, for $n=m$, we obtain

$$\frac{d\mu_m}{d\lambda} = -\langle \psi_m | z \cos \theta | \psi_m \rangle. \tag{20}$$

On the other hand, for $n \neq m$ and $\mu_n \neq \mu_m$,

$$\langle \psi_n | \frac{d}{d\lambda} | \psi_m \rangle = -\frac{\langle \psi_n | z \cos \theta | \psi_m \rangle}{\mu_m - \mu_n}.$$

Therefore, applying completeness of the $|\psi_m\rangle$ basis, we obtain

$$\frac{d}{d\lambda} | \psi_m \rangle = -\sum_{n \neq m} |\psi_n\rangle \frac{\langle \psi_n | z \cos \theta | \psi_m \rangle}{\mu_m - \mu_n} + c |\psi_m\rangle, \tag{21}$$

where

$$c = \langle \psi_m | \frac{d}{d\lambda} | \psi_m \rangle.$$

However, a phase factor can be chosen such that $c=0$. We can see this in the following way. First, note that $\langle \psi_m | \psi_m \rangle = 1$ implies

$$\left[\frac{d}{d\lambda} \langle \psi_m | \right] | \psi_m \rangle + \langle \psi_m | \frac{d}{d\lambda} | \psi_m \rangle = c^* + c = 0;$$

then c is purely imaginary. Now, for small $\delta\lambda$, we have that

$$\psi_m(\lambda + \delta\lambda) = \psi_m(\lambda) + \delta\lambda \frac{d\psi_m}{d\lambda} + O(\delta\lambda^2).$$

Since we can choose a phase factor of $|\psi_m(\lambda + \delta\lambda)\rangle$ so that the product $\langle \psi_m(\lambda) | \psi(\lambda + \delta\lambda) \rangle$ is real [15], we conclude that c must be zero. Substituting in Eq. (21), we obtain

$$\frac{d}{d\lambda} | \psi_m \rangle = -\sum_{n \neq m} |\psi_n\rangle \frac{\langle \psi_n | z \cos \theta | \psi_m \rangle}{\mu_m - \mu_n}. \tag{22}$$

To obtain the second derivative of the quasienergies μ_m with respect to λ, from Eqs. (20) and (22) we have

$$\frac{d^2\mu_m}{d\lambda^2} = -\frac{d}{d\lambda} \langle \psi_m | z \cos \theta | \psi_m \rangle$$

$$= -\left[\frac{d}{d\lambda} \langle \psi_m | \right] z \cos \theta | \psi_m \rangle - \langle \psi_m | z \cos \theta \frac{d}{d\lambda} | \psi_m \rangle$$

$$= \sum_{n \neq m} \frac{\langle \psi_n | z \cos \theta | \psi_m \rangle^*}{\mu_m - \mu_n} \langle \psi_n | z \cos \theta | \psi_m \rangle$$

$$+ \sum_{n \neq m} \langle \psi_m | z \cos \theta | \psi_n \rangle \frac{\langle \psi_n | z \cos \theta | \psi_m \rangle}{\mu_m - \mu_n}$$

$$= 2 \sum_{n \neq m} \frac{\langle \psi_n | z \cos \theta | \psi_m \rangle^2}{\mu_m - \mu_n}.$$

In numerical explorations, we observe avoided crossings of the quasienergies, together with dramatic changes in the Floquet states. Consider the case where two quasienergies μ_m and μ_n are very close; in the last derivation, we can approximate the sum with only the two closest quasienergies:

$$\frac{d^2\mu_m}{d\lambda^2} \approx 2 \frac{|\langle \psi_n | z \cos \theta | \psi_m \rangle|^2}{\mu_m - \mu_n} \approx -\frac{d^2\mu_n}{d\lambda^2}.$$

This implies that $\mu_n + \mu_m$ behaves linearly with respect to λ around the avoided crossing. Close to an avoided crossing of μ_m and μ_n, we have

$$\frac{d}{d\lambda} \langle \psi_n | z \cos \theta | \psi_m \rangle = \left[\frac{d}{d\lambda} \langle \psi_n | \right] z \cos \theta | \psi_m \rangle$$

$$+ \langle \psi_n | z \cos \theta \frac{d}{d\lambda} | \psi_m \rangle$$

$$= -\sum_{p \neq n} \frac{\langle \psi_p | z \cos \theta | \psi_n \rangle^*}{\mu_n - \mu_p} \langle \psi_p | z \cos \theta | \psi_m \rangle$$

$$- \langle \psi_n | z \cos \theta \sum_{p \neq m} |\psi_p\rangle \frac{\langle \psi_p | z \cos \theta | \psi_m \rangle}{\mu_m - \mu_p}$$

$$\approx \frac{\langle \psi_n | z \cos \theta | \psi_m \rangle}{\mu_m - \mu_n} \left(-\frac{d\mu_m}{d\lambda} + \frac{d\mu_n}{d\lambda} \right).$$

In the last step, we kept only the terms for $p=m$ in the first sum, and $p=n$ in the second sum, which are the most significant contributions close to the avoided crossing $\mu_n \approx \mu_m$.

Therefore, we obtain the following differential equation:

$$\frac{d}{d\lambda} \langle \psi_n | z \cos \theta | \psi_m \rangle = -\frac{\langle \psi_n | z \cos \theta | \psi_m \rangle}{\mu_m - \mu_n} \left[\frac{d}{d\lambda} (\mu_m - \mu_n) \right],$$

which implies

$$\langle \psi_n | z \cos \theta | \psi_m \rangle (\mu_m - \mu_n) = \text{const}. \tag{23}$$

The last identity shows a common behavior at avoided crossings: if two quasienergies μ_n and μ_m are very close to each other, the matrix element $\langle \psi_n | z \cos \theta | \psi_m \rangle$ increases, in order to preserve the product (23). As a consequence, from Eq. (22),

$$\frac{d}{d\lambda} | \psi_m \rangle \approx -|\psi_n\rangle \frac{\text{const.}}{(\mu_m - \mu_n)^2}.$$

This implies dramatic changes in the Floquet states at avoided crossings when the parameter λ is varied.

B. Quasienergies as a function of ω

When the frequency field ω is varied, a similar analysis can be done. Proceeding in a similar way as for the variation with respect to λ, we can obtain an equation analog of Eq. (20):

$$\frac{d\mu_m}{d\omega} = \langle \psi_m | I | \psi_m \rangle,$$

where I is the additional action variable of the Floquet Hamiltonian (18). Also,
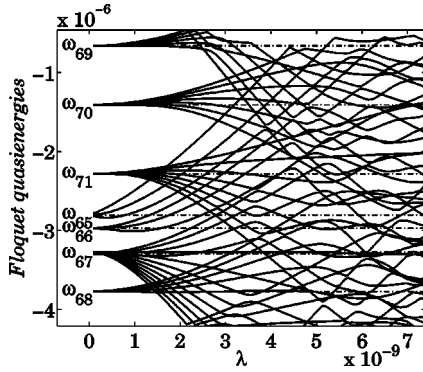
FIG. 9. Floquet quasienergies μ_m for varying λ. The frequency of the field is fixed $\omega=\omega_{65}-\omega_{64}$. The range of the field strength λ is 0.5 V/cm–38.5 V/cm. The dotted lines are the values of the unperturbed energies (modulo ω). Avoided crossings produce dramatic turns of the quasienergies.

$$\frac{d}{d\omega}|\psi_m\rangle = -\sum_{n\neq m}|\psi_n\rangle\frac{\langle\psi_n|I|\psi_m\rangle}{\mu_m-\mu_n}.$$

Furthermore, it can be shown that $\langle\psi_m|I|\psi_m\rangle(\mu_m-\mu_n)$ =const. These equations show that avoided crossings of the quasienergies as a function of ω are also accompanied by sudden changes in the Floquet states.

VI. SELECTION RULES FOR AVOIDED CROSSINGS

The behavior of the quasienergies as a function of the field strength λ is illustrated in Fig. 9. For this computation, we consider excited states with quantum number $m=63$. Since m is fixed, only states with principal quantum numbers $n=64,65,\ldots$ and $l=63,\ldots,n-1$ interact [see Eq. (10)]. The choice of quantum number $m=63$ produces 45 interacting states for values of $n=64,\ldots,72$. The field frequency is fixed $\omega=\omega_{65}-\omega_{64}$, and λ varies from 1×10^{-11} to 7.5×10^{-9} (0.05 to 38.5 V/cm). We observe that for small λ, the Floquet quasienergies split from the unperturbed energies (appearing in the figure as ω_n mod ω). This can be interpreted as the ac *or dynamic Stark shift* [5,6]. As λ increases, we observe apparent crossings and avoided crossings. There is no reason *a priori* to rule out crossings of the quasienergies in Eq. (19); degenerate Floquet states might exist for some values of λ. In our numerical experiments, we found that some selection rules apply for these degeneracies, at least for small λ. This will be explained in the next example.

A. Quasienergy crossings, avoided crossings, the eigenvectors, and selection rules, as λ varies

In Fig. 10, we present an example showing crossings and avoided crossings. For this case, the field frequency is $\omega=\omega_{67}-\omega_{64}$, and λ varies. A total of 45 states were integrated, for principal quantum numbers $n=64,\ldots,72$ and $m=63$. The labeling of the quasienergies is arbitrary; in this case, we plotted 11 of the 45 computed quasienergies: $\mu_1, \mu_2, \ldots, \mu_{11}$.

For small λ, we observe that the quasienergies corresponding to $n=65$ and $n=72$ get closer; producing some
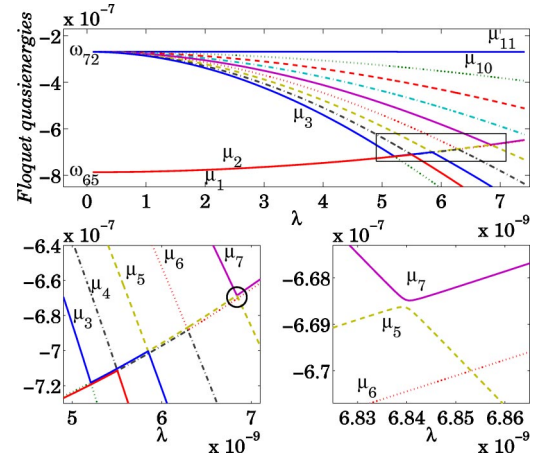

FIG. 10. (Color online) Floquet quasienergies μ_m for varying λ. The frequency of the field is $\omega=\omega_{67}-\omega_{64}$. We observe that some crossings occur as well as avoided crossings. See text for more details.

crossings and some avoided crossings. This can be appreciated in the second and third panel of Fig. 10. We can observe that the crossings and avoided crossings alternate. The explanation of this fact will be described below, from observing the behavior of the eigenvectors as a function of λ. Note also that, for this choice of ω, we have $\omega_{72}-\omega_{65}\approx2\omega$.

Recall that, at $t=0$, the Floquet states are obtained as an expansion in terms of unperturbed states, with the coefficients given by the components of the eigenvectors [see Eqs. (13) and (15)]. We observe that for small λ there is one large eigenvector component close to 1, and the rest are close to 0; the Floquet states are very close to the unperturbed states. As λ increases, more components of the eigenvectors increase in value; hence, the Floquet states are expanded in terms of more unperturbed states. When an avoided crossing occurs, the components of the eigenvectors also feature dramatic changes, as we showed analytically in Sec. V.

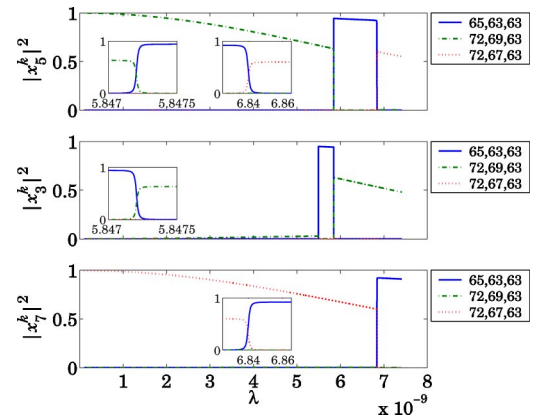In Fig. 11, we plot the square modulus of some components of three eigenvectors, corresponding to the quasiener-

FIG. 11. (Color online) Squared modulus of some components of the eigenvectors x_m^k as a function of λ, corresponding to Floquet quasienergies μ_5, μ_6, and μ_7 in Fig. 10. The eigenvector components suffer dramatic changes at avoided crossings, the components showed are $k=65,63,63$, $k=72,69,64$, and $k=72,67,63$.

gies μ_7, μ_3, and μ_5 of Fig. 10; they are associated with quasienergies featuring avoided crossings. In each case, the components correspond to the unperturbed states $|72,69,63\rangle$, $|65,63,63\rangle$, and $|72,67,63\rangle$. Around the avoided crossing at $\lambda=6.84\times10^{-9}$, we can see that the component $k=65,63,63$ of the eigenvector x_5 goes quickly to zero (see second inset in the first panel). At that point, the same component of the eigenvector x_7 increases by the same amount (see inset in the third panel). This behavior is reproduced in all components of the eigenvectors involved in avoided crossings. Exactly for a value of λ for which an avoided crossing occurs, the eigenvectors have two or more important components; these are the coefficients for the unperturbed states, and as a result, the Floquet states are a superposition of several unperturbed states. This results in probability exchange between the unperturbed states involved. On the other hand, when a crossing occurs, the components of the eigenvectors do not reflect any sudden change, neither do the Floquet states, and no probability transition takes place.

As mentioned above, for small values of λ, the Floquet states are still close to unperturbed states, so they can be easily identified with the $|n,l,m\rangle$ states. This leads to the following selection rule for this choice of ω: the quasienergies that have avoided crossings correspond to states for which the difference in quantum number l is even; then probability exchange is possible only when $l-l'$ is even. If the difference in l is odd, the quasienergies cross, and there is no probability exchange. This selection rule is related to the particular resonance. In this case, we have that $\omega_{72}-\omega_{65}\approx2\omega$; this avoided crossing involves a two-photon transition between states in $n=65$ and $n=72$. We note that this transition is slow, the period of the Rabi oscillation, from Eq. (17), is $\omega/(\mu_7-\mu_5)\approx66,188$ field periods.

B. Transitions from the ground state as ω varies

The selection rules also appear when we study probability transitions as a function of the field frequency ω. To illustrate this, first we study transitions from the ground state to low levels (small n). We show that crossings and avoided crossings of the quasienergies occur for values of ω satisfying closely a resonance equation of the form $\omega_k-\omega_1=N\omega$.

When ω varies, keeping λ fixed, crossings and avoided crossings of the quasienergies are observed, as we show in Fig. 12 for low quantum numbers $n=1,\ldots,5$ and $m=0$. In this example, the varying frequency is $\omega=\omega_0/d$, with $\omega_0=\omega_3-\omega_1$, and the denominator d varies continuously between 0.1 and 5. The field frequency is fixed as $\lambda=0.006$. The quasienergies are represented in the figure as a function of d. We plotted, with dotted lines, the curves $\omega_1+N\omega$ as well as the lines for the unperturbed energies $\omega_2,\ldots,\omega_5$. The points where these lines and curves intersect, represent an unperturbed resonance (i.e., a resonance for the unperturbed energies) of the form $\omega_k-\omega_1=N\omega$. As we can expect, the crossings and avoided crossings of the quasienergies occur for values of ω close to an unperturbed resonance, i.e., $\omega\approx(\omega_k-\omega_1)/N$.

We observe that the quasienergies have split from the unperturbed energies, this is clearly seen in the second panel of
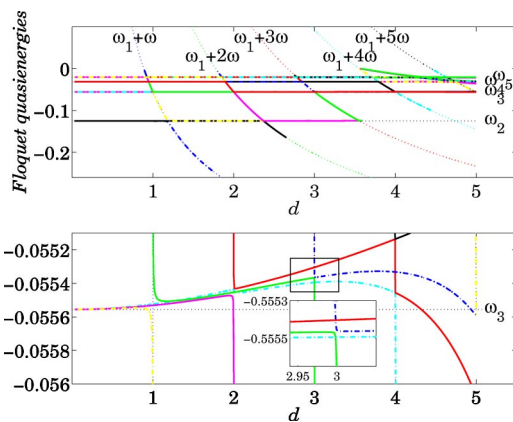

FIG. 12. (Color online) Floquet quasienergies varying the field frequency ω; $\lambda=0.006$ fixed. The varying frequency is $\omega=\omega_0/d$, with $\omega_0=\omega_3-\omega_1$. The states correspond to $m=0$ and principal quantum numbers $n=1,2,\ldots,5$. The dotted curves in the background correspond to the resonances for the unperturbed energies. In the second panel the splitting of the $n=3$ energy level is shown (dynamic Stark shift).

Fig. 12, where a zoom of the quasienergies close to ω_3 is shown. In the inset, we can see one avoided crossing and several crossings. The avoided crossing occurs for $\omega\approx(\omega_3-\omega_1)/3$. Hence, this avoided crossing reflects a 3-photon transition between the ground state $n=1$ and a state in $n=3$. To study this transition, we compute the eigenvectors corresponding to the quasienergies in the avoided crossing, as a function of d. Only two eigenvector components have high values, they are the coefficients of the unperturbed states $|1,0,0\rangle$ and $|3,1,0\rangle$. Our computations show that these eigenvector components change quickly around the avoided crossing. Therefore, for this value of ω, there is a 3-photon transition between the states $|1,0,0\rangle$ and $|3,1,0\rangle$. The transition is of the Rabi type. As before [see Eq. (17)], we can calculate the period of the Rabi oscillation, as $\omega/(\mu_9-\mu_8)=1602T$.

Selection rules. These computations confirm the selection rules obtained in the preceding section. For these small values of λ, the Floquet states are close to the unperturbed states. Therefore, only one component of the eigenvectors is close to 1 and the rest are close to zero; this permits us to associate a label n,l,m to the Floquet states. Avoided crossings occur only when the difference in l quantum number $(l-l')$ is even for N even (in the equation $\omega_j-\omega_k=N\omega$) or when $l-l'$ is odd for N odd. And, since avoided crossings produce dramatic exchange between the components of the Floquet states, probability exchange is possible only between states for which there is an avoided crossing. Therefore, these are the selection rules for probability transitions between unperturbed states.

C. Transitions between excited states: The tuning of λ and ω

When considering excited state, the situation is more complicated due to the small separation of the unperturbed energies. The resonant frequencies of the form $\omega=\omega_j-\omega_k$ are small, then the quasienergies are very close together since
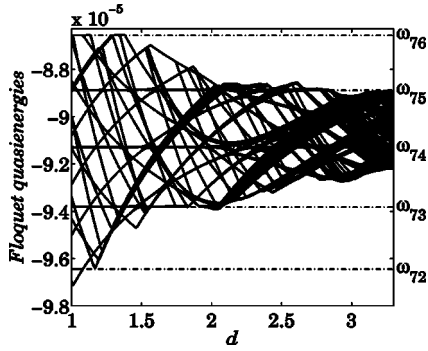
FIG. 13. Floquet quasienergies varying the field frequency. $\lambda = 2 \times 10^{-9}$ is fixed (≈ 10.3 V/cm). The varying frequency is $\omega = \omega_0/d$, with $\omega_0 = \omega_{67} - \omega_{64}$. The states correspond to $m = 63$ and principal quantum numbers $n = 64, 65, \ldots, 80$.

they are obtained modulo ω. Therefore, more crossings and avoided crossings occur. This can be observed in Fig. 13. For this case, we considered states with quantum numbers $n = 64, \ldots, 80$; $m = 63$; and $l = 63, \ldots, n-1$. The varying frequency is $\omega = \omega_0/d$, with $\omega_0 = \omega_{67} - \omega_{64} = 1.068 \times 10^{-5}$, and the denominator d is dimensionless, taken between 1 and 3.2. The field strength parameter $\lambda = 2 \times 10^{-9}$ is fixed (≈ 10.3 V/cm). The quasienergies are plotted as a function of the denominator d. In dotted lines, some unperturbed frequencies are shown (right vertical axis). For this kind of computation, some extra work is necessary in order to obtain a good representation of the quasienergies. Since the quasienergies are obtained modulo ω, it is common to obtain discontinuous curves that seem senseless. However, we can add multiples of ω as needed to obtain continuous curves. When this is done, we observe both crossings and avoided crossings, corresponding to all kinds of resonance relations.

The values of ω and λ can be both tuned to achieve the desired transition and the rate of the Rabi oscillation. In Fig. 14, we observe that as ω varies, and the quasienergies feature an avoided crossing, also the coefficients c_m in the expansion
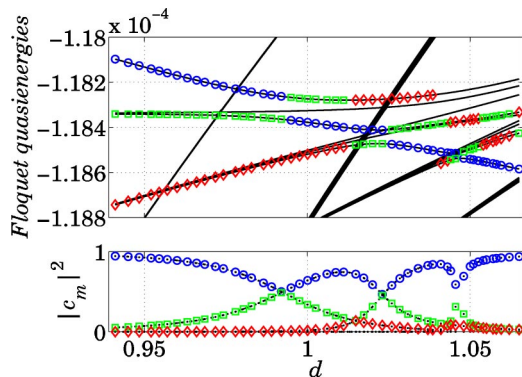

FIG. 14. (Color online) Above, the three main Floquet quasienergies in the evolution of the state $|64, 63, 63\rangle$ are marked with circles, squares, and diamonds (in that order). At the bottom, the coefficients c_m of the Floquet states [as in expansion (14)]. This was calculated for varying field frequency $\omega = \omega_0/d$, with $\omega_0 = \omega_{65} - \omega_{64}$. $\lambda = 3 \times 10^{-10}$ fixed (≈ 1.6 V/cm). The states correspond to $m = 63$ and principal quantum numbers $n = 64, 65, \ldots, 80$.
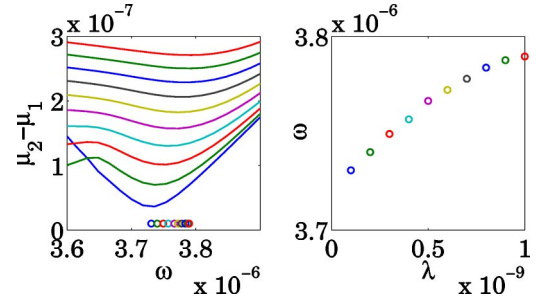

FIG. 15. (Color online) In the first panel, the quasienergy difference $\mu_2 - \mu_1$ is plotted as a function of ω. Each curve corresponds to a different value of λ. The minimum in each curve is an avoided crossing related to the 1-photon transition between $n = 64$ and $n = 65$. The avoided crossing for each λ occurs at a different value of ω. These values of ω are depicted in the second panel.

(14) have quick changes. In the first panel, we mark in circles, squares, and diamonds the three main quasienergies (in that order) involved in the evolution of the initial state $|64, 63, 63\rangle$. The corresponding coefficients c_m of the Floquet states are shown in the second panel. Exactly at an avoided crossing, there are two (or at most three) significant coefficients c_m. Then, for the choice of ω producing an avoided crossing, the evolution of the initial state is a superposition of two or three Floquet states only.

Our calculations show that the values of ω that produce avoided crossings depend on the value of λ. In Fig. 15 the difference between two quasienergies μ_1 and μ_2, related to a 1-photon transition between $n = 64$ and $n = 65$, is plotted as a function of ω, and for different values of λ. As λ increases, the difference $\mu_2 - \mu_1$ also increases. For each fixed value of λ, we computed the value of ω producing the minimum, i.e., the avoided crossing. As we can expect, the values of ω are close to $\omega_{65} - \omega_{64} = 3.7271 \times 10^{-6}$. But, as λ increases, the value of ω producing the avoided crossing also increases, as can be observed in the second panel of Fig. 15. This computation also allows us to determine the implications of the choice of parameters in probability transitions. For the parameters λ, ω in Fig. 15, and for $|64, 63, 63\rangle$ as the initial condition, the main Floquet states are expanded in terms of the unperturbed states $|64, 63, 63\rangle$ and $|65, 64, 63\rangle$; but as λ increases, also the states $|66, 65, 63\rangle$, $|67, 66, 63\rangle$, etc., have significant coefficients. That is, if a new level n is involved, only the state with $l = n-1$ gains probability. Notice that this is the probability of a multiphoton transition to that state. As higher n levels have nonzero probability, there is higher probability of multiphoton ionization.

VII. CONCLUSIONS

The problem of multiphoton transition of the Rydberg atom in a strong, long-wavelength microwave field is described with a nonperturbative approach, providing a time-dependent solution of the Schrödinger equation. Using the Goeppert-Mayer gauge transformation, the time-dependent solution is obtained in both the length gauge (electric dipole Hamiltonian) and the velocity gauge (standard vector potential coupling Hamiltonian).

The dynamics is reduced to a system of ordinary differential equations for the coefficients $a_k(t)$ of the expansion of the time-dependent solution in terms of the unperturbed states (that is, the atomic states, when no radiation field is present). Coupling between states in different levels, and between substates within an n level, results in spreading of probability, for which many states need to be included in the analysis.

The auxiliary equations for the coefficients $a_k(t)$ form a linear, time-periodic system. The numerical integration of the auxiliary equations, together with the Goeppert-Mayer gauge transformation, provide exact time evolution of the transition probabilities between unperturbed states in the presence of the radiation field. The choice of field strength λ and frequency ω determine the extent and rate of the transition. Multiphoton transitions can be observed, for $\omega \approx (\omega_k - \omega_j)/N$, but the choice of ω depends on the value of λ. Note that, in previous work [16], the same approach was used to show that there are no multiphoton transitions of the simple harmonic oscillator in a radiation field.

The introduction of Floquet analysis of the auxiliary equations (a system of time-periodic ODE's) proved to be an excellent tool to analyze transition probabilities. From the Floquet solutions and multipliers of the auxiliary equations, we obtain Floquet states and quasienergies of the quantum system. The expansion of the initial condition in terms of Floquet states (at $t=0$) is enough to know exactly the time evolution of probabilities. For cases when the initial condition is expanded in terms of mainly two Floquet states, the probability transition is of Rabi type between two unperturbed states, and it is possible to obtain the rate of transition. We show, however, that other coupled states also gain probability, therefore the strict reduction to a two-level system is not justified.

The Floquet analysis of transitions between excited Rydberg states $(n > 60)$ showed that the probability transitions are very sensitive to changes in the parameters λ and ω. We show, analytically and numerically, that the probability transitions are associated with multiple crossings and avoided crossings of the quasienergies, as the parameters vary. The expressions for the derivatives of the Floquet states and quasienergies with respect to the parameters λ and ω are derived analytically from the Floquet Hamiltonian, which permit us to show that avoided crossings are accompanied by sudden changes of the Floquet states. Therefore, avoided crossings produce probability transitions between the states involved. When a quasienergy crossing occurs (up to the numerical accuracy), the Floquet states do not show any sudden change, and no probability transition takes place.

We observe that the quasienergy crossings and avoided crossings are determined by the unperturbed states involved, obeying selection rules for probability transitions. For small λ, if the difference in quantum number l has the same parity as the N-multiphoton process, then there is an avoided crossing. That is, for a choice of $\omega \approx (\omega_k - \omega_j)/N$, an avoided quasienergy crossing is produced only when the corresponding Floquet states are expanded in terms of states with $l - l'$ odd for N odd or $l - l'$ even for N even. Therefore, probability transition is only possible between unperturbed states that satisfy this selection rule.

The value of ω that produces an avoided crossing depends on the field strength λ. As λ increases, the value of ω at the avoided crossing also increases. For large λ, the choice of ω producing an avoided crossing results in Floquet states that are not close anymore to unperturbed states; they have many components corresponding to unperturbed states with higher n and $l=n-1$. This means that the probability spreads to states of the form $|n, n-1, m\rangle$, with larger n. As a consequence, there is an increase in multiphoton ionization probability.

For large values of λ, more avoided quasienergy crossings appear and they may even overlap. Also, most Floquet states are expanded in terms of many unperturbed states. The mixing of unperturbed states results in large diffusion of probability among many states. In this process, it is hard to differentiate the exchange of probability in an n shell from the exchange between different levels. In Ref. [2], some intriguing experiments showed that intrashell dynamics was responsible for enhancement of ionization probability. Some numerical and analytic work [7,12,13] has been done to study the effect of intrashell dynamics. However, our analysis shows that the intrashell dynamics cannot be isolated from transitions between different levels, since these two processes occur together and for all neighboring states for strong enough fields.

APPENDIX: SECULARITIES OF THE AUXILIARY EQUATION

Note that by defining $b_k = a_k e^{i\omega_k t}$, we can write Eq. (9) as

$$\frac{d}{dt} b_k = \frac{i\lambda}{2} \sum_{j=1}^{\infty} Z_{kj} (e^{i(\omega_k - \omega_j + \omega)t} + e^{i(\omega_k - \omega_j - \omega)t}) b_j,$$

where $Z_{kj} = \langle \phi_k | r \cos \theta | \phi_j \rangle$.

Denoting the Laplace transform of $b_k(t)$ as $\mathcal{L}(b_k) = \hat{b}_k(s)$, and noting that $\mathcal{L}((d/dt)b_k) = s\hat{b}_k(s) - b_k(0)$, the previous equation can be transformed to

$$\hat{b}_k(s) = \frac{1}{s} b_k(0) + \frac{i\lambda}{2s} \sum_{j=1}^{\infty} Z_{kj}\{\hat{b}_j[s - i(\omega_k - \omega_j + \omega)]$$
$$+ \hat{b}_j[s - i(\omega_k - \omega_j - \omega)]\}.$$

The first iterate of this formula produces

$$\hat{b}_k(s) = \frac{1}{s}b_k(0) + \frac{i\lambda}{2}\sum_{j_1} Z_{kj_1}\frac{1}{s}\left(\frac{b_{j_1}(0)}{s - i(\omega_k - \omega_{j_1} + \omega)} + \frac{b_{j_1}(0)}{s - i(\omega_k - \omega_{j_1} - \omega)} \right)$$

$$+ \left(\frac{i\lambda}{2}\right)^2 \sum_{j_1}\sum_{j_2} Z_{kj_1}Z_{j_1j_2}\frac{1}{s}\left(\frac{\hat{b}_{j_2}[s - i(\omega_k - \omega_{j_2} + 2\omega)] + \hat{b}_{j_2}[s - i(\omega_k - \omega_{j_2})]}{s - i(\omega_k - \omega_{j_1} + \omega)} \right.$$

$$\left. + \frac{\hat{b}_{j_2}[s - i(\omega_k - \omega_{j_2})] + \hat{b}_{j_2}[s - i(\omega_k - \omega_{j_2} - 2\omega)]}{s - i(\omega_k - \omega_{j_1} - \omega)} \right).$$

We can continue to iterate this formula to obtain an asymptotic solution of the form

$$\hat{b}_k(s) = \frac{1}{s}b_k(0) + \sum_{n=1}^{\infty}\left(\frac{i\lambda}{2}\right)^n \sum_{j_1}\sum_{j_2}\cdots\sum_{j_n} Z_{kj_1}Z_{j_1j_2}\cdots Z_{j_{n-1}j_n}\frac{1}{s}\left\{ \sum_{p_1=0}^{1}\sum_{p_2=0}^{1}\cdots\sum_{p_n=0}^{1}\prod_{r=1}^{n}\frac{b_{j_n}(0)}{s - i\left[\omega_k - \omega_{j_r} + \sum_{l=1}^{r}(1-2p_l)\omega\right]} \right\}.$$

This equation has secularities whenever ω is in resonance:

$$\omega_m - \omega_{j_r} = \pm N\omega,$$

N a positive integer. Therefore, the choice of resonant ω will result in probability transition. Although computing the inverse Laplace transform is very complicated, the asymptotic formula gives heuristic ideas of how the solution will behave up to a certain order. For instance, up to first order in λ, only frequencies of the driving force satisfying $\omega_j - \omega_k = \pm\omega$ will produce a secularity. Therefore a multiphoton process of the form $\omega_j - \omega_k = \pm N\omega$ will require higher order in λ (field strength) to be observed.

---

[1] P. M. Koch, in *The Ubiquity of Chaos*, edited by Saul Krasner (AAAS, Washington, D.C., 1990), Chap. 8.

[2] P. M. Koch, E. J. Galvez, and S. A. Zelazny, Physica D **131**, 90 (1999).

[3] E. J. Galvez, P. M. Koch, D. Richards, and S. A. Zelazny, Phys. Rev. A **61**, 060101 (2000).

[4] M. Goeppert-Mayer, Ann. Phys. (Leipzig) **9**, 273 (1931); P. W. Milonni, Phys. Rep. **25C**, 1 (1976); P. I. Richards, Phys. Rev. **73**, 254 (1948); A restricted version of this transformation for the case of a constant magnetic field in both space and time appeared see W. E. Lamb, *ibid.* **85**, 259 (1952); B. R. Johnson, J. O. Hirschfelder, and K.-H. Yang, Rev. Mod. Phys. **55**, 109 (1983).

[5] F. H. M. Faisal, *Theory of Multiphoton Processes*, 1st ed. (Plenum Press, New York, 1987).

[6] B. W. Shore, *The Theory of Coherent Atomic Excitation*, 1st ed. (Wiley, New York, 1990).

[7] V. N. Ostrovsky and E. Horsdal-Pedersen, Eur. Phys. J. D **23** 1 (2003); **23**, 15 (2003).

[8] J. H. Shirley, Phys. Rev. **138**, B979 (1965).

[9] K. F. Milfeld and R. E. Wyatt, Phys. Rev. A **27**, 72 (1982).

[10] S. I. Chu, Adv. At. Mol. Phys. **21**, 197 (1985).

[11] K. Wang and S. I. Chu, Phys. Rev. A **39**, 1800 (1989).

[12] F. Robicheaux, E. Oks, A. L. Parker, and T. Uzer, J. Phys. B **35**, 4613 (2002).

[13] E. Oks and T. Uzer, J. Phys. B **33**, 1985 (2000).

[14] D. I. Blochinzew, Phys. Z. Sowjetunion **4**, 501 (1933).

[15] C. Cohen-Tannoudji, B. Diu, and F. Laloë, *Quantum Mechanics*, 1st ed. (Wiley, New York, 1977).

[16] R. F. Fox and L. V. Vela-Arevalo, Phys. Rev. A **66**, 053402 (2002).

[17] R. F. Fox and P. Jung, Phys. Rev. A **57**, 2339 (1998); see also M. Thorwart, P. Reimann, P. Jung, and R. F. Fox, Phys. Lett. A **239**, 233 (1998); Chem. Phys. **235**, 61 (1998).

[18] D. Hone, R. Ketzmerick, and W. Kohn, Phys. Rev. A **56**, 4045 (1997).

[19] E. Merzbacher, *Quantum Mechanics*, 3rd ed. (Wiley, New York, 1998).

[20] H. A. Bethe and E. E. Salpeter, *Quantum Mechanics of One- and Two-Electron Atoms*, 1st ed. (Plenum, New York, 1977).

[21] *Handbook of Mathematical Functions*, 9th ed., edited by M. Abramowitz and I. A. Stegun (Dover, New York, 1972).

[22] L. V. Vela-Arevalo (unpublished).

[23] M. Farkas, *Periodic Motions*, 1st ed. (Springer-Verlag, New York, 1994).